Dynamics of matrix-free Ca^{2+} in cardiac mitochondria: two components of Ca^{2+} uptake and role of phosphate buffering

An-Chi Wei,[2] Ting Liu,[1] Raimond L. Winslow,[2] and Brian O'Rourke[1]

[1]Division of Cardiology, Department of Medicine, and [2]Institute for Computational Medicine, Department of Biomedical Engineering, Johns Hopkins University, Baltimore, MD 21205

Mitochondrial Ca^{2+} uptake is thought to provide an important signal to increase energy production to meet demand but, in excess, can also trigger cell death. The mechanisms defining the relationship between total Ca^{2+} uptake, changes in mitochondrial matrix free Ca^{2+}, and the activation of the mitochondrial permeability transition pore (PTP) are not well understood. We quantitatively measure changes in $[Ca^{2+}]_{out}$ and $[Ca^{2+}]_{mito}$ during Ca^{2+} uptake in isolated cardiac mitochondria and identify two components of Ca^{2+} influx. $[Ca^{2+}]_{mito}$ recordings revealed that the first, MCU_{mode1}, required at least 1 µM Ru360 to be completely inhibited, and responded to small Ca^{2+} additions in the range of 0.1 to 2 µM with rapid and large changes in $[Ca^{2+}]_{mito}$. The second component, MCU_{mode2}, was blocked by 100 nM Ru360 and was responsible for the bulk of total Ca^{2+} uptake for large Ca^{2+} additions in the range of 2 to 10 µM; however, it had little effect on steady-state $[Ca^{2+}]_{mito}$. MCU_{mode1} mediates changes in $[Ca^{2+}]_{mito}$ of 10s of µM, even in the presence of 100 nM Ru360, indicating that there is a finite degree of Ca^{2+} buffering in the matrix associated with this pathway. In contrast, the much higher Ca^{2+} loads evoked by MCU_{mode2} activate a secondary dynamic Ca^{2+} buffering system consistent with calcium-phosphate complex formation. Increasing P_i potentiated $[Ca^{2+}]_{mito}$ increases via MCU_{mode1} but suppressed $[Ca^{2+}]_{mito}$ changes via MCU_{mode2}. The results suggest that the role of MCU_{mode1} might be to modulate oxidative phosphorylation in response to intracellular Ca^{2+} signaling, whereas MCU_{mode2} and the dynamic high-capacity Ca^{2+} buffering system constitute a Ca^{2+} sink function. Interestingly, the trigger for PTP activation is unlikely to be $[Ca^{2+}]_{mito}$ itself but rather a downstream byproduct of total mitochondrial Ca^{2+} loading.

The Journal of General Physiology

INTRODUCTION

Ca^{2+} is the central signaling molecule for cardiac excitation-contraction coupling, and its uptake by mitochondria plays a fundamental role in the regulation of ATP production (McCormack et al., 1990; Demaurex and Distelhorst, 2003; Maack and O'Rourke, 2007; Szabadkai and Duchen, 2008). In addition, the extent of mitochondrial Ca^{2+} uptake during metabolic stress determines whether the myocyte lives or dies, owing to the activation of the permeability transition pore (PTP; Crompton, 1999). Although PTP activation is unequivocally linked to total mitochondrial Ca^{2+} load, it is presently unclear how much Ca^{2+} is free or bound in the mitochondrial matrix during PTP activation, as well as how much Ca^{2+} is required to maintain energy balance.

Mitochondrial matrix free Ca^{2+} ($[Ca^{2+}]_{mito}$) is determined by the balance between Ca^{2+} uptake, extrusion, and buffering. Ca^{2+} uptake is driven by the electrochemical Ca^{2+} gradient and is mediated by a mitochondrial Ca^{2+}-selective uniporter (MCU; Gunter and Pfeiffer, 1990), a Ruthenium red (or its potent subcomponent, Ru360)–sensitive ion channel, whose selectivity is determined by nanomolar affinity Ca^{2+} binding to the pore, with an open probability that is voltage dependent (Kirichok et al., 2004). In single-channel mitoplast patch recordings of cardiac mitochondria, two different mitochondrial Ca^{2+} channels, mCU1 and mCU2, with different gating properties and Ru360 sensitivity, were observed (Michels et al., 2009). Two independent groups have recently reported that the molecular identity of the MCU pore is the protein product of the gene CCDC109A (Baughman et al., 2011; De Stefani et al., 2011). Knockdown of this gene suppresses the major component of mitochondrial Ca^{2+} uptake in cultured cells and in the liver (Baughman et al., 2011) and reconstitution of the protein forms Ca^{2+} channels in lipid bilayers (De Stefani et al., 2011). Nevertheless, in addition to the major component of MCU, other potential Ca^{2+} uptake pathways have been noted in mitochondria, including the rapid mode (RaM) of Ca^{2+} uptake (Sparagna et al., 1995; Buntinas et al., 2001) and the mitochondrial ryanodine receptor (mRyR; Beutner et al., 2001; Ryu et al., 2010). The relative importance of each Ca^{2+} uptake pathway, with respect to function, has not yet been determined.

Correspondence to Brian O'Rourke: bor@jhmi.edu

Abbreviations used in this paper: MCU, mitochondrial Ca^{2+}-selective uniporter; mNCE, mitochondrial Na^+/Ca^{2+} exchanger; PTP, permeability transition pore; RaM, rapid mode.

The Rockefeller University Press $30.00
J. Gen. Physiol. Vol. 139 No. 6 465–478
www.jgp.org/cgi/doi/10.1085/jgp.201210784

Ca^{2+} extrusion in cardiac mitochondria is determined primarily by the mitochondrial Na^+/Ca^{2+} exchanger (mNCE; Crompton et al., 1977). Its molecular identity is thought to be an ancestral member of the Na^+/Ca^{2+} exchanger family, NCLX, a transporter capable of exchanging Ca^{2+} for either Na^+ or Li^+ (Palty et al., 2010). The mNCE plays an important role in modulating the steady-state balance between extra- and intramitochondrial Ca^{2+} in isolated mitochondria (Wei et al., 2011), and disruption of this equilibrium in conditions of cellular Na^+ overload associated with cardiac disease can impact pyridine nucleotide redox and ROS balance in cardiac cells (Maack et al., 2006; Liu and O'Rourke, 2008; Kohlhaas et al., 2010). A minor component of mitochondrial Ca^{2+} efflux is also contributed by the mitochondrial PTP (Wei et al., 2011), which has been proposed to serve as a Ca^{2+} relief valve for mitochondria (Gunter and Pfeiffer, 1990). Disruption of this mechanism can have diverse functional consequences in vivo (Elrod et al., 2010).

The least well understood, but perhaps most important, determinant of $[Ca^{2+}]_{mito}$ is the Ca^{2+} buffering system of the mitochondrial matrix, consisting of both fixed and dynamic buffering mechanisms. The rapid formation of complexes between Ca^{2+} and phosphate (P_i) in mitochondria, described almost 50 yr ago, has been shown to be of major importance in determining how much Ca^{2+} can be accumulated into mitochondria, as well as how much $[Ca^{2+}]_{mito}$ changes in response to total Ca^{2+} taken up (Nicholls and Chalmers, 2004; Chinopoulos and Adam-Vizi, 2010). In fact, in the presence of P_i, but not acetate, as the accompanying permeant anion, mitochondria are capable of sequestering enormous amounts of total Ca^{2+} (>1 M), while maintaining $[Ca^{2+}]_{mito}$ in the low micromolar range, as determined in isolated mitochondria loaded with matrix free Ca^{2+} indicators (Davis et al., 1987; Lukács and Kapus, 1987; Gunter et al., 1988; Lukács et al., 1988; Saavedra-Molina et al., 1990; Walajtys-Rhode et al., 1992; Chalmers and Nicholls, 2003). Interestingly, this range of $[Ca^{2+}]_{mito}$, <5 µM, appears to be the range over which key Ca^{2+}-sensitive mitochondrial enzymes are regulated (Denton et al., 1980; McCormack et al., 1990; Walajtys-Rhode et al., 1992).

In cardiac mitochondria, although many studies have investigated rates of Ca^{2+} uptake, efflux, and PTP activation in isolated mitochondria and intact cells using various methods, the dynamics and quantitative determinants of changes in $[Ca^{2+}]_{mito}$ are incompletely understood. Here, we use matrix-loaded fura-FF, a ratiometric Ca^{2+} indicator with an intermediate Ca^{2+}-binding affinity, to quantitatively examine changes in $[Ca^{2+}]_{mito}$ while simultaneously monitoring extramitochondrial Ca^{2+} and $\Delta\Psi_m$ in isolated guinea pig heart mitochondria. The results indicate that two components of mitochondrial Ca^{2+} uptake are present: one which mediates a large, rapid change in $[Ca^{2+}]_{mito}$ in response to small additions of extramitochondrial Ca^{2+} (MCU_{mode1}), and another which mediates the stereotypical slow, lower affinity, Ca^{2+} uptake pathway (MCU_{mode2}) which is capable of taking up large amounts of Ca^{2+} but leads to relatively small changes in $[Ca^{2+}]_{mito}$. Although MCU_{mode2} is completely blocked by 100 nM Ru360, MCU_{mode1} has a lower inhibitor affinity, requiring 1 µM Ru360 for complete inhibition. The differential responses of $[Ca^{2+}]_{mito}$ to Ca^{2+} entry via the two different pathways can be explained by a two component buffer system comprised of both static Ca^{2+} buffers and dynamic Ca^{2+} buffering by P_i, which enters in parallel with large amplitude Ca^{2+} influx. The findings have important implications with respect to the physiological regulation of oxidative phosphorylation by Ca^{2+}, as well as for the activation of the PTP, which, remarkably, is shown to be uncorrelated with $[Ca^{2+}]_{mito}$.

MATERIALS AND METHODS

Mitochondria were isolated from adult guinea pig hearts on ice using a homogenization method previously described (Aon et al., 2010). In brief, the heart tissue was homogenized in 75 mM sucrose, 225 mM mannitol, 1 mM HEPES, and 1 mM EGTA, pH 7.4, with 0.1 mg/ml bacterial proteinase type XXIV (Sigma-Aldrich). The homogenate was centrifuged at 480 *g* for 5 min at 4°C, and the supernatant was centrifuged at 7,700 *g* for 10 min. The mitochondrial pellet was washed twice at 7,700 *g* for 5 min and resuspended in sucrose-based isolation solution with 20 µM EGTA to ~10–20 mg mitochondrial protein/ml (protein concentration was determined by BCA assay). During the experiments, ~0.6 mg of isolated mitochondria was suspended in 2 ml potassium-based buffer solution composed of: 137 mM KCl, 20 µM EGTA, 20 mM HEPES, and 5 mM glutamate/malate (G/M), with or without 2 mM KH_2PO_4 at pH 7.15.

Multiple mitochondrial parameters, including mitochondrial inner membrane potential ($\Delta\Psi_m$) extra- and intramitochondrial Ca^{2+} concentrations, and mitochondrial light scattering, were simultaneously monitored in a stirred cuvette using a fluorometer (QuantaMaster; Photon Technology International) at room temperature. $\Delta\Psi_m$ was monitored by the dual-excitation ratiometric method with the fluorescent probe tetramethylrhodamine methyl ester (TMRM; 300 nM) at excitations of 546 and 573 nm and emission at 590 nm (Scaduto and Grotyohann, 1999). Mitochondrial 90° light scattering was monitored at 540 nm excitation. The fluorescent Ca^{2+} indicator Calcium green 5N (CaGreen; Invitrogen) was used to monitor extramitochondrial Ca^{2+} ($[Ca^{2+}]_{out}$), with excitation and emission wavelengths at 505 and 535 nm. Quantitative measurements of $[Ca^{2+}]_{mito}$ were made with the dual-excitation ratiometric Ca^{2+} indicator fura-FF, loaded into the isolated mitochondria as the fura-FF-AM form (20 µM for 30 min at room temperature; washed two to three times with sucrose-based isolation buffer). The fura-FF signal was calibrated in mitochondria treated with the Ca^{2+} ionophore 4-bromo-A23187 (2 µM; Deber et al., 1985; Nicholls and Chalmers, 2004) in the presence of 5 µg/ml oligomycin and 5 µM FCCP to allow equilibration between intra- and extramitochondrial calcium (Wan et al., 1989; Chalmers and Nicholls, 2003; Andrienko et al., 2009; Fig. 1). The calibration curve was established according to the following equation (Grynkiewicz et al., 1985):

$$[Ca^{2+}] = K_d' \beta \frac{(R - R_{min})}{(R_{max} - R)},$$

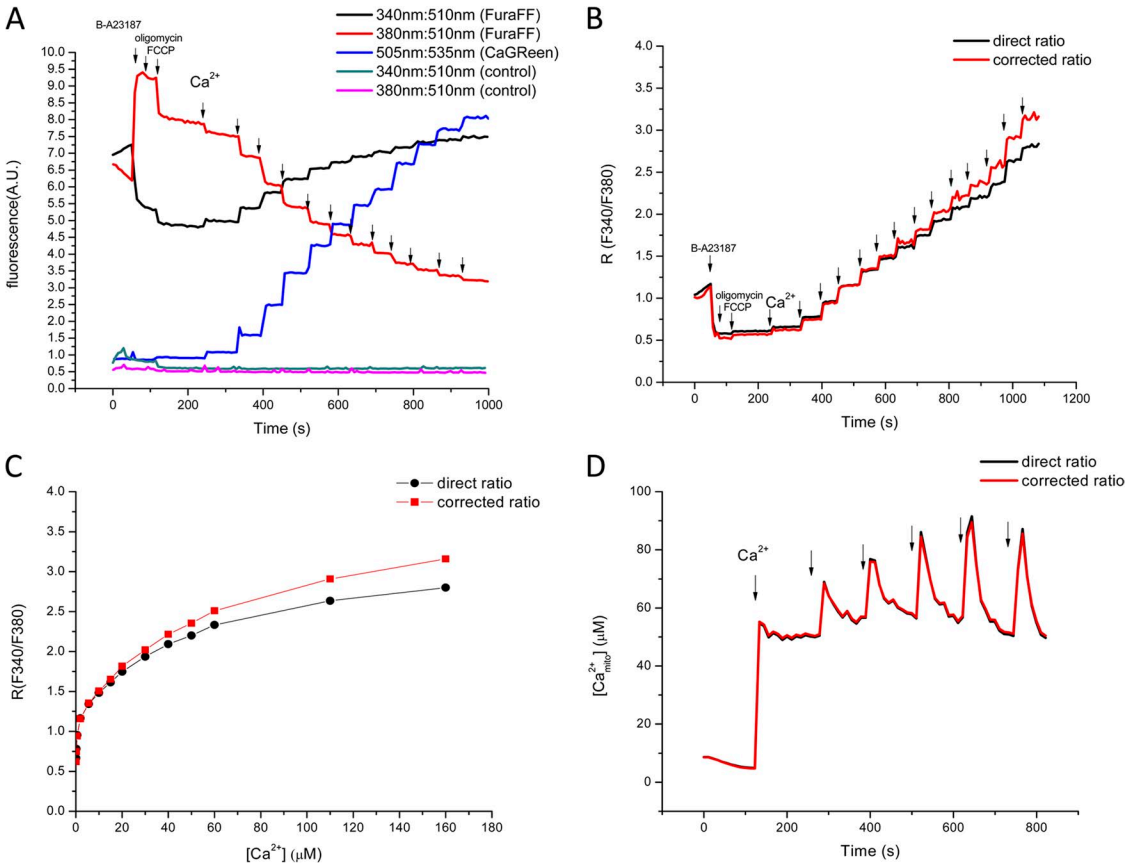

Figure 1. Calibration of fura-FF signals. (A) Fluorescence recordings of mitochondria in the presence or absence of fura-FF loading (340:510 nm ex:em and 380:510 nm FuraFF or control, respectively) along with $[Ca^{2+}]_{out}$ (CaGreen: 505:535 nm ex:em). The Ca^{2+} signals were calibrated with multiple additions of 5 µM Ca^{2+} in the presence of the ionophore, 2 µM 4-bromo-A23187, 5 µg/ml oligomycin, and 5 µM FCCP. (B) The excitation ratio for fura-FF was calculated with (red) or without (black) correction for autofluorescence. (C) $[Ca^{2+}]_{mito}$ was determined after fitting the calibration curve to the equation $[Ca^{2+}] = Kd'\beta\ (R - R_{min})/(R_{max} - R)$. The values obtained were $R_{max} = 3.2$, $R_{min} = 0.5$, $K_d' = 10.7$, $\beta = 2.5$ without autofluorescence correction (black); $R_{max} = 3.7$, $R_{min} = 0.5$, $K_d' = 12.7$, $\beta = 2.75$ for corrected ratio (red). (D) $[Ca^{2+}]_{mito}$ in intact mitochondria after multiple additions of Ca^{2+} (15.3 µM first addition, 5.7 µM for subsequent additions) show that autofluorescence correction had little effect on the calculated $[Ca^{2+}]_{mito}$.

where R is the ratio of 510-nm emission intensities for excitation at 340 and 380 nm. K_d' is the apparent Ca-fura-FF dissociation constant, and β is the fluorescence intensity ratio for Ca^{2+}-free and Ca^{2+}-saturated fura-FF excited at 380 nm. R_{max} and R_{min} are R values for Ca^{2+}-saturated and Ca^{2+}-free fura-FF. The calibration was done for fura-FF–loaded mitochondria for each day's experiment (example shown in Fig. 1). Ratios of background-uncorrected and background-corrected fura-FF fluorescence signal at 340 and 380 nm excitation were fitted to the Grynkiewicz equation (Fig. 1, B and C). Autofluorescence values, and their changes upon Ca^{2+} addition, were relatively small compared with the fura-FF fluorescence intensities (Fig. 1 A, teal and magenta traces) and $[Ca^{2+}]_{mito}$ calculated from calibration curves with or without subtraction of autofluorescence showed no significant differences (Fig. 1 D). Therefore, autofluorescence corrections were not necessary, and were not made, in the subsequent experiments. The method for calibrating the extramitochondrial calcium signal (CaGreen) was as described previously (Wei et al., 2011).

In the Results and Figure Legends, Ca^{2+} additions to the cuvette are those calculated using the online version of WEBMAXC (http://maxchelator.stanford.edu/webmaxc/webmaxcE.htm). Taking into account the presence of 20 µM EGTA in the experimental solution, this corresponded to free Ca^{2+} changes in the cuvette of 0.011, 0.2, 0.55, 2, 5.7, and 15.3 µM for additions of 1, 10, 15, 20, 25, and 35 µM Ca^{2+}, respectively. Because other low-affinity Ca^{2+} buffers in the solution, such as glutamate and malate, were not included in this calculation, these numbers tend to overestimate the free Ca^{2+} change for larger Ca^{2+} additions, explaining discrepancies in the direct measurements of initial $[Ca^{2+}]_{out}$ using calibrated CaGreen signals. Mitochondrial matrix calcium buffering, i.e., the relationship between the total Ca^{2+} taken up by mitochondria and the change in $[Ca^{2+}]_{mito}$, was expressed as the ratio of bound/free Ca^{2+} and was examined in the presence of different anions, including P_i (0.1–10 mM), arsenate (As_i; 2 mM), or vanadate (V_i; 2 mM). Cyclosporin A (CsA; 1 µM) was used to shift the threshold for activation of the PTP to a higher Ca^{2+} range to study Ca^{2+} dynamics over a wide range of mitochondrial Ca^{2+} loads. The figures show representative responses for each experiment; however, every experiment was repeated at least three times with a similar result (see Fig. S1 for an example of the range of statistical variability of the response).

Online supplemental material

Fig. S1 shows the mean and standard error of the response of $[Ca^{2+}]_{mito}$ to large Ca^{2+} additions ($n = 4$ experiments). Fig. S2 shows the lack of a ryanodine effect on mitochondrial Ca^{2+} for a

single Ca^{2+} addition. Fig. S3 shows Na^+/Ca^{2+} exchanger effects on mitochondrial Ca^{2+} with different concentrations of Na^+ and in the presence of the inhibitor CGP37157. Online supplemental material is available at http://www.jgp.org/cgi/content/full/jgp.201210784/DC1.

RESULTS

In Fig. 2 (top), simultaneous recordings of $[Ca^{2+}]_{out}$ (green traces), $[Ca^{2+}]_{mito}$ (black traces), and $\Delta\Psi_m$ (red traces) are shown superimposed for large (Fig. 2, A–D) or small (Fig. 2, E–H) Ca^{2+} additions to the cuvette (from a starting $[Ca^{2+}]_{out}$ of ~0.100 µM before the first addition). Immediately evident is the fact that two components of the mitochondrial Ca^{2+} response are present. For the series of larger Ca^{2+} additions in Fig. 2 A, although the first Ca^{2+} addition (15.3 µM) evoked a large increase in $[Ca^{2+}]_{mito}$ to ~50 µM, subsequent additions (5.7 µM each) caused a transient increase (amplitude 10–20 µM) in $[Ca^{2+}]_{mito}$, followed by a decline back to the same 50 µM steady-state matrix concentration. Moreover, after the sixth Ca^{2+} addition, this steady-state $[Ca^{2+}]_{mito}$ begins to decrease after each pulse (to ~20 µM), suggesting an increase in the matrix Ca^{2+} buffer capacity (changes in matrix volume, as assessed by light scattering, could not account for these changes in $[Ca^{2+}]_{mito}$, compare Fig. 8). $\Delta\Psi_m$ depolarized by 5–10 mV with each Ca^{2+} addition and recovered back to 180 mV as extramitochondrial Ca^{2+} (and MCU flux, which follows the electrochemical gradient for Ca^{2+}) returned to a low level. Comparing the change in matrix free Ca^{2+} (expressed as nmols/mg mitochondrial protein assuming 1 µl/mg mitochondrial volume; Fig. 2 B) to the total amount of Ca^{2+} taken up from the bath (ΣCa^{2+}_{uptake}; Fig. 2 C) allowed us to calculate the ratio of bound/free Ca^{2+} (Fig. 2 D), illustrating how the buffer capacity dramatically increases after the first Ca^{2+} addition.

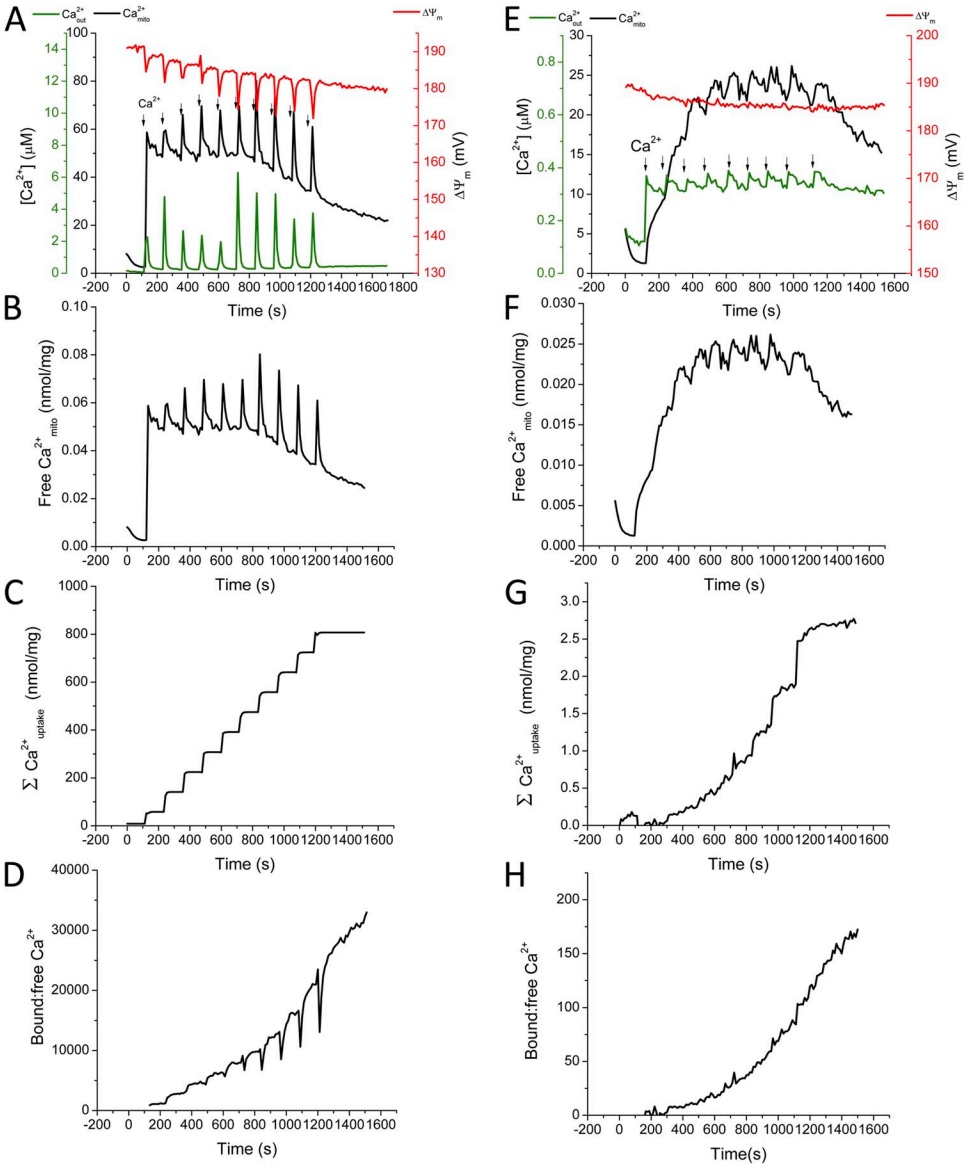

Figure 2. $[Ca^{2+}]_{mito}$ (black), $[Ca^{2+}]_{out}$ (green), and $\Delta\Psi_m$ (red) responses to large or small Ca^{2+} additions in isolated guinea pig heart mitochondria. (A–D) Ca^{2+} additions were as follows: 15.3 µM Ca^{2+} first addition, 5.7 µM for each subsequent addition. (E–H) Ca^{2+} additions were as follows: 0.2 µM Ca^{2+} first addition, 0.011 µM for each subsequent addition. Corresponding calculated values of free Ca^{2+}_{mito} expressed in nmol/mg, total ΣCa^{2+} taken up, and the bound/free Ca^{2+} ratio are shown for large (A–D) or small (E–H) additions. $[Ca^{2+}]_{mito}$ and $[Ca^{2+}]_{out}$ were monitored with Calcium green and fura-FF simultaneously. Experimental solution was the standard KCl-based buffer with 5 mM NaCl, 5 mM G/M, 1 mM KH_2PO_4, 20 µM EGTA, and 1 µM CsA. 300 nM TMRM was used to monitor $\Delta\Psi_m$ ratiometrically.

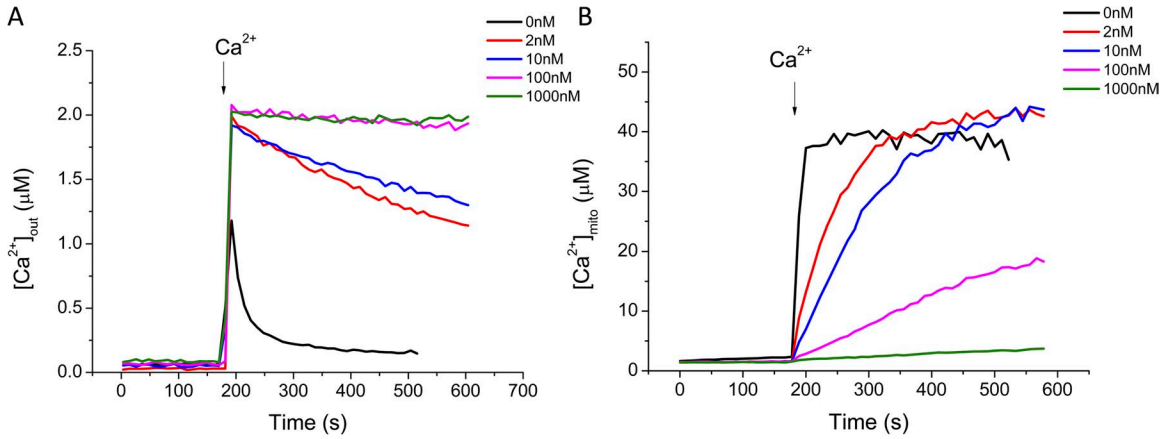

Figure 3. Concentration dependence of Ru360 inhibition of mitochondrial Ca^{2+} uptake. Fura-FF–loaded mitochondria were preincubated with 0 (black), 2 (red), 10 (blue), 100 (magenta), or 1,000 nM (green) Ru360 in the standard KCl-based buffer with 2 mM KH_2PO_4, 5 mM G/M, 5 mM NaCl, 10 μM CGP37157, 1 μM CsA, and 2.5 μM thapsigargin. 2 μM free Ca^{2+} was added to initiate mitochondrial Ca^{2+} uptake and $[Ca^{2+}]_{out}$ (A) and $[Ca^{2+}]_{mito}$ (B) were monitored simultaneously.

The initial rapid jump in $[Ca^{2+}]_{mito}$ (MCU_{mode1}), which reached completion well before the end of the major slow uptake phase of the uniporter (MCU_{mode2}), prompted us to explore the $[Ca^{2+}]_{mito}$ response to a much lower range of Ca^{2+} concentrations.

Fig. 2 E shows that adding 0.2 μM Ca^{2+} first allows one to resolve the kinetics of the initial high-affinity Ca^{2+} uptake. $[Ca^{2+}]_{mito}$ increased over the course of 100 s (as compared with the <10-s increase for the 15.3-μM addition in Fig. 2 A) and responded in a stepwise fashion for two subsequent additions of 0.01 μM each. Six more 0.01 μM Ca^{2+} additions evoked transient increases in $[Ca^{2+}]_{mito}$ but little change in the steady-state $[Ca^{2+}]_{mito}$ until the ninth addition, when the steady state actually began to decline. $\Delta\Psi_m$ decreased by only 3 mV (188 to 185mV) after the first Ca^{2+} addition but did not change for subsequent additions (Fig. 2 E). Interestingly, despite the 100-fold lower amount of total Ca^{2+} loaded into the mitochondria in the small (Fig. 2 G) versus large (Fig. 2 C) Ca^{2+} addition experiments, the steady-state $[Ca^{2+}]_{mito}$, in both cases, settled into a range between 15 and 20 μM, demonstrating that matrix Ca^{2+} buffering dynamically responds over a very wide range. This is clearly evident when one compares the changes in matrix free Ca^{2+} (Fig. 2, B and F) with the total Ca^{2+} taken up by the mitochondria (Fig. 2, C and G), expressed as the ratio of bound/free Ca^{2+} (Fig. 2, D and H). This ratio spanned from ∼3 to 30,000 over the range of Ca^{2+} additions examined.

We next examined the properties of MCU_{mode1} in greater detail for an initial Ca^{2+} addition of 2 μM. CGP-37157, cyclosporin A, and thapsigargin were also included in the experimental solution to inhibit possible Ca^{2+} fluxes through the mNCE, PTP, and the sarcoplasmic reticular Ca^{2+} ATPase, respectively. Ru360 is a derivative of Ruthenium red that potently inhibits mitochondrial Ca^{2+} uptake with a K_D of ∼1.3 nM (Ying et al., 1991). In the absence of Ru360, $[Ca^{2+}]_{mito}$ (Fig. 3 B, black trace) increased rapidly after the Ca^{2+} addition and then reached a plateau, even though extramitochondrial Ca^{2+} decreased continuously over 50–100 s (Fig. 3 A, black trace). At Ru360 concentrations of 2 and 10 nM (Fig. 3 B, red and blue traces), the rate of rise of MCU_{mode1} was slowed but its plateau was unchanged. In contrast, MCU_{mode2} was markedly inhibited (the initial rate of decline of $[Ca^{2+}]_{out}$ decreased by almost 95%) at 10 nM Ru360 (Fig. 3 A, blue trace) and was completely blocked by 100 nM Ru360 (Fig. 3 A, magenta trace). MCU_{mode1}, in contrast, was only partially inhibited by 100 nM Ru360, and 1 μM Ru360 was required for complete inhibition (Fig. 3 B).

The greater sensitivity of MCU_{mode2} to inhibition by Ru360 allowed us to investigate the Ca^{2+} dependence of MCU_{mode1} with MCU_{mode2} largely inhibited. Fig. 4 shows the $[Ca^{2+}]_{mito}$ response to Ca^{2+} additions in the range of 0.2 to 5.7 μM Ca^{2+} in the absence (Fig. 4 A) and presence (Fig. 4 B) of 10 nM Ru360. With MCU_{mode2} almost completely inhibited by Ru360, as indicated by the near step-like changes in cuvette Ca^{2+} upon Ca^{2+} addition (Fig. 4 B, bottom), the rate of rise of MCU_{mode1} increased as a function of Ca^{2+} and the plateau level of $[Ca^{2+}]_{mito}$ increased to ∼40 μM for additions of 2 and 5.7 μM (Fig. 4 B, top). Remarkably, although much more total Ca^{2+} uptake occurred with both MCU_{mode1} and MCU_{mode2} active in the absence of Ru360 (Fig. 4 A, bottom), the change in plateau $[Ca^{2+}]_{mito}$, presumably mediated only by MCU_{mode1}, was very similar, reaching a plateau of ∼40 μM free Ca^{2+} (Fig. 4 A, top). The rate of rise of MCU_{mode1} was ∼10-fold faster in the absence of 10 nM Ru360; however, the Ca^{2+} dependence of the rate was similar. Steady-state $\Delta\Psi_m$ was maintained at close to 185 mV during these experiments (unpublished data). The results indicate that MCU_{mode1} underlies the largest change in $[Ca^{2+}]_{mito}$ after a Ca^{2+} addition to isolated

cardiac mitochondria, whereas the large amount of Ca^{2+} taken up via MCU_{mode2} is almost entirely buffered.

The experiments shown in Fig. 5 were designed to test (1) whether the initial jump in $[Ca^{2+}]_{mito}$ mediated by MCU_{mode1} could be reset and repeated if cuvette Ca^{2+} was lowered by EGTA addition, and (2) whether Ca^{2+} efflux from the compartment reported by fura-FF was mediated by the mNCE. Isolated mitochondria were first subjected to a single addition of Ca^{2+} (2 µM) to initiate mitochondrial Ca^{2+} uptake. EGTA was then added to decrease $[Ca^{2+}]_{out}$ back to the nM range (~100 nM) and a second Ca^{2+} addition was made (4 µM). In the absence of extramitochondrial Na^+, $[Ca^{2+}]_{out}$ declined with a time course similar to the experiments described in the previous paragraphs and $[Ca^{2+}]_{mito}$ again showed a rapid increase via MCU_{mode1} to reach a plateau (Fig. 5 A). EGTA addition resulted in a rapid decrease in $[Ca^{2+}]_{out}$ but $[Ca^{2+}]_{mito}$ remained elevated (Fig. 5 A). A second Ca^{2+} addition effected a transient in $[Ca^{2+}]_{out}$ similar to the first addition; however, instead of a stepwise increase in $[Ca^{2+}]_{mito}$ the second pulse evoked a spike and decay response of $[Ca^{2+}]_{mito}$. Apparently, when $[Ca^{2+}]_{mito}$ is already elevated, additional Ca^{2+} entering via MCU is buffered after a transient response. In contrast, in the presence of Na^+, both $[Ca^{2+}]_{out}$ and $[Ca^{2+}]_{mito}$ decline after EGTA addition (Fig. 5 B). A second Ca^{2+} addition in this case evokes a $[Ca^{2+}]_{mito}$ response similar to the first pulse, i.e., a rapid rise and plateau. Collectively, these results show that the rapid rise in $[Ca^{2+}]_{mito}$ via MCU_{mode1} is best observed when $[Ca^{2+}]_{out}$ is increased from the nanomolar to the micromolar range, and when the total mitochondrial Ca^{2+} load is low. Moreover, the Ca^{2+} compartment filled via MCU_{mode1} is emptied via mNCE, confirming that it is either the same compartment that is filled by MCU_{mode2}, or it has Ca^{2+} efflux pathways identical to the latter.

The same two-pulse protocol evoked two increases in $[Ca^{2+}]_{mito}$ that plateaued after ~100 s with MCU_{mode2} completely blocked with 100 nM Ru360 (Fig. 5 C). This residual uptake was likely to be mediated by MCU_{mode1}, whose kinetics were slowed by 100 nM Ru360, in accordance with the data shown in Fig. 3 B. Finally, the same protocol was applied in a more physiological condition in the presence of 2 mM MgATP (free Mg^{2+} was calculated to be 0.467 mM, which is close to that

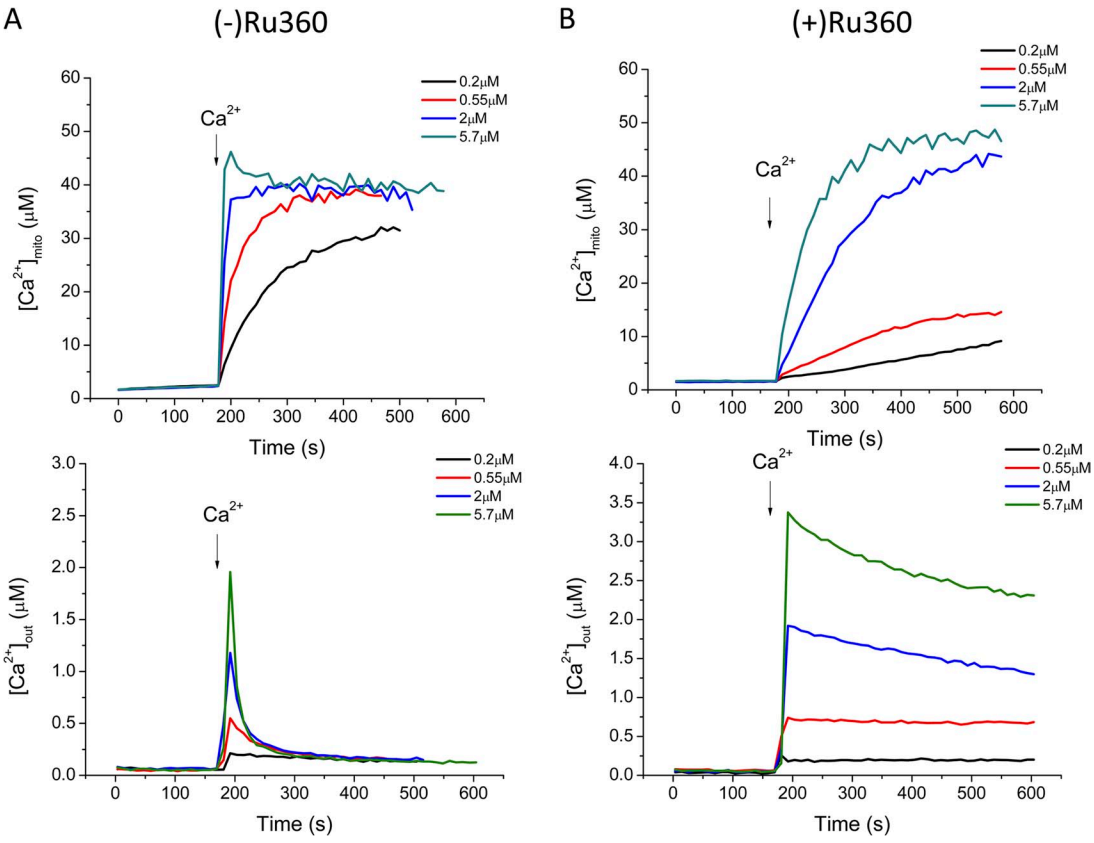

Figure 4. Calcium dependence of mitochondrial Ca^{2+} uptake in the absence (A) and presence (B) of 10 nM Ru360. $[Ca^{2+}]_{out}$ and $[Ca^{2+}]_{mito}$ were monitored during mitochondrial Ca^{2+} uptake initiated by Ca^{2+} additions ranging from 0.2 (black), to 0.55 (red), to 2 (blue), to 5.7 µM (green). 10 nM Ru360 largely eliminated MCU_{mode2} (see $[Ca^{2+}]_{out}$ in bottom panels) but only partially inhibited MCU_{mode1} ($[Ca^{2+}]_{mito}$ response in top panels). Standard KCl-based buffer with 2 mM KH_2PO_4, 5 mM G/M, 5 mM NaCl, 10 µM CGP, 1 µM CsA, and 2.5 µM thapsigargin.

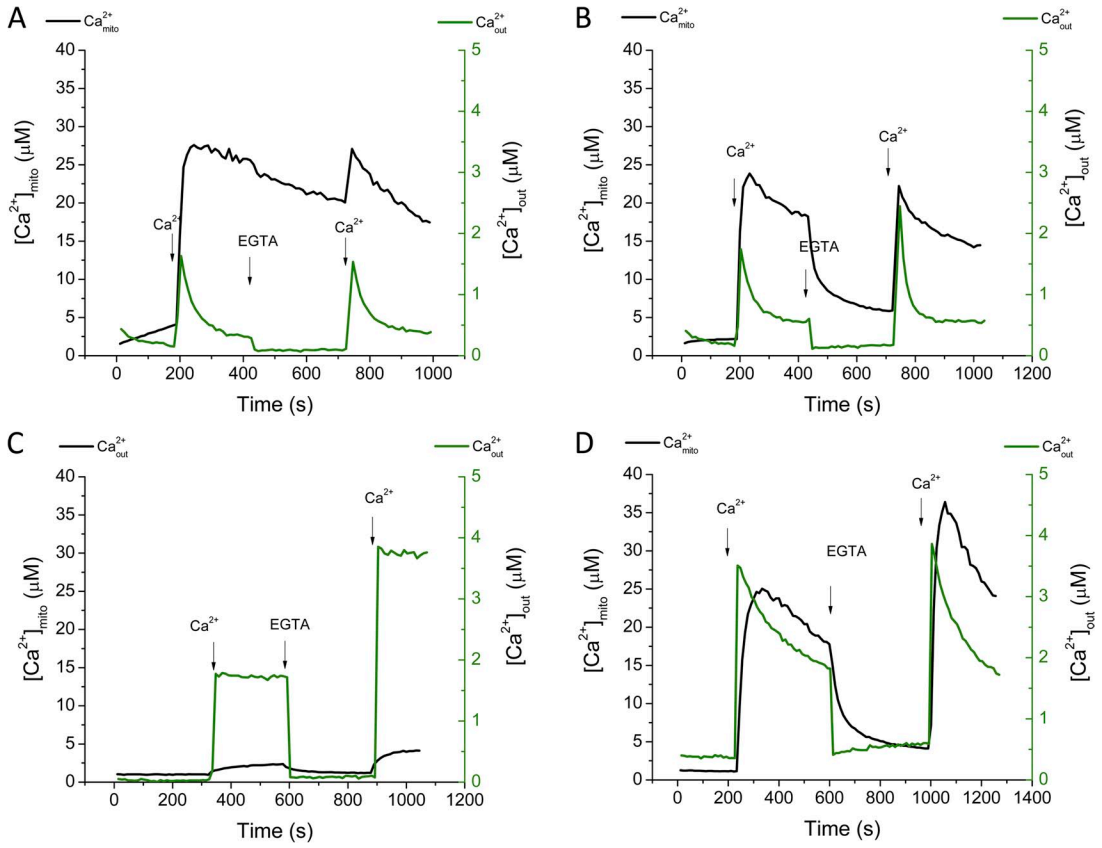

Figure 5. Resetting of $[Ca^{2+}]_{mito}$ (black) for two Ca^{2+} additions. 2 μM Ca^{2+} was first added to initiate mitochondrial Ca^{2+} uptake. 25 μM EGTA was added to decrease the extramitochondrial calcium concentration ($[Ca^{2+}]_{out}$, green) to the submicromolar range, and another 4 μM Ca^{2+} was added to evoke a second $[Ca^{2+}]_{mito}$ response. A decrease in $[Ca^{2+}]_{mito}$ upon lowering $[Ca^{2+}]_{out}$ occurred only in the presence of Na^{+}. Conditions: (A) zero NaCl; (B) 15 mM NaCl; (C) 15 mM NaCl plus 100 nM Ru360; (D) 15 mM NaCl plus 2 mM MgATP.

present in the cytoplasm). In the presence of MgATP, the rates of mitochondrial Ca^{2+} uptake via MCU_{mode1} and MCU_{mode2} were both decreased (Fig. 5 D), but the Na^{+}-dependent Ca^{2+} efflux rate and qualitative responses to the sequential pulses were similar to those in the absence of MgATP (compare Fig. 5 B).

The slowing of the Ca^{2+} uptake rate with MgATP could be attributed to the increased Mg^{2+} present in the solution (Fig. 6). The physiological Mg^{2+} concentration in cytosol is ∼0.1–0.8 mM (Szanda et al., 2009) and Mg^{2+} is known to have inhibitory effects on mitochondrial Ca^{2+} uptake (Crompton et al., 1975; Bragadin et al., 1979). The effects of Mg^{2+} (from 0.1 to 1.0 mM) on mitochondrial Ca^{2+} uptake and $[Ca^{2+}]_{mito}$ were compared for both small and large Ca^{2+} additions. The mitochondrial Ca^{2+} uptake rate and $[Ca^{2+}]_{mito}$ were minimally affected for additions of 15 μM Ca^{2+} (Fig. 6, A–C); however, with smaller Ca^{2+} additions (first Ca^{2+} addition, 0.2 μM; subsequent, 0.011 μM each), Mg^{2+} slowed mitochondrial Ca^{2+} uptake (Fig. 6, D and E). Decreased uptake was indicated by higher $[Ca^{2+}]_{out}$ and lower $[Ca^{2+}]_{mito}$ in the presence of high Mg^{2+}. The finding that Mg^{2+} inhibition can be overcome at high Ca^{2+} suggests that Mg^{2+} is competitive with respect to Ca^{2+} flux through the MCU.

The rapid buffering of $[Ca^{2+}]_{mito}$ during large increases in total mitochondrial Ca^{2+} evident in the preceding experiments prompted us to investigate the effects of changing the anion concentration on matrix Ca^{2+} dynamics. Because the formation of calcium phosphate complexes is thought to be the major mitochondrial Ca^{2+} buffering reaction (Nicholls and Chalmers, 2004), we examined the effects of varying P_i over the range of 0.1 to 10 mM for both large and small Ca^{2+} additions. In 0.1 mM P_i, the first large Ca^{2+} addition (15.3 μM) increased $[Ca^{2+}]_{mito}$ immediately to ∼50 μM (Fig. 7 A; black trace), and subsequent Ca^{2+} additions (5.7 μM each) induced transients in $[Ca^{2+}]_{mito}$ with increasing amplitudes of >100 μM. Nevertheless, $[Ca^{2+}]_{mito}$ returned to a matrix setpoint of 50 μM after each transient. Ca^{2+} additions in the presence of 0.1 mM P_i evoked deeper and more prolonged depolarizations in $\Delta\Psi_m$ (Fig. 7 A; red trace) than those observed for 1 mM (Fig. 7 B) or 10 mM (Fig. 7 C) P_i, increasing in amplitude from 20 to 40 mV with each subsequent addition. The overall rate of mitochondrial Ca^{2+} uptake was accelerated in 1 mM (Fig. 7 B) and 10 mM (Fig. 7 C) P_i, as compared with the rate in 0.1 mM P_i, and the rate of return of $[Ca^{2+}]_{mito}$ to the matrix Ca^{2+} setpoint was accelerated. Moreover, the

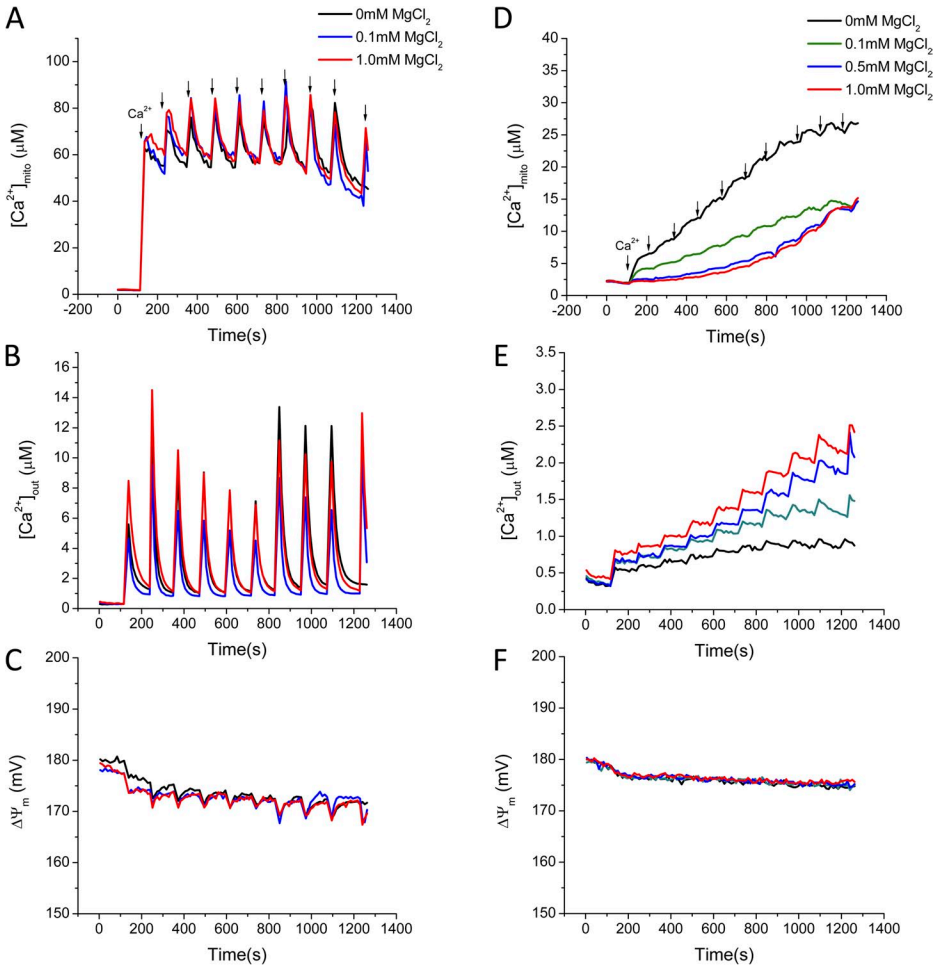

Figure 6. Effect of Mg^{2+} on the regulation of mitochondrial Ca^{2+}. (A–C) Large Ca^{2+} additions (Ca^{2+} additions were 15.3 µM each) in the presence of zero (black), 0.1 (blue), or 1 mM (red) $MgCl_2$. (D–F) Small Ca^{2+} additions (first Ca^{2+} addition 0.2 µM, subsequent 0.011 µM each) with 0 (black), 0.1 (green), 0.5 (blue), and 1 mM (red) $MgCl_2$.

$[Ca^{2+}]_{mito}$ setpoint achieved was lowered to 30 µM in 1 mM Pi and to 11 µM in 10 mM Pi by the end of the protocol. $\Delta\Psi_m$ was well maintained in both 1 and 10 mM Pi (Fig. 7, B and C). Thus, the Ca^{2+} buffering action of P_i facilitates the regulation of $[Ca^{2+}]_{mito}$ down to low levels in the face of very high mitochondrial Ca^{2+} loads and preserves the energy state of the mitochondria.

For small Ca^{2+} additions (0.2 µM first, with subsequent additions of 0.011 µM each), P_i had a different effect on $[Ca^{2+}]_{mito}$ (Fig. 7, D and E). In this case, increasing P_i from 0.1 to 1 to 10 mM markedly enhanced the rise in $[Ca^{2+}]_{mito}$ associated with each Ca^{2+} addition and $[Ca^{2+}]_{mito}$ was not regulated down to the low levels observed after larger Ca^{2+} additions. The enhanced Ca^{2+} uptake at high P_i was indirectly confirmed by the fact that $[Ca^{2+}]_{out}$ was also observed to be lower in 10 mM P_i (Fig. 7 D, bottom). With MCU_{mode2} inhibited with 10 nM Ru360, the potentiating effect of P_i on mitochondrial Ca^{2+} uptake for the high-affinity uptake pathway was still present (Fig. 7 E). These results illustrate the complexity of the mitochondrial matrix Ca^{2+} buffering system, which depends on the amplitudes and rates of entry of both Ca^{2+} and P_i.

Finally, the effect of varying the chemical nature of the buffering anion was explored by comparing the effects of P_i with those of the P_i analogues, vanadate (V_i), or arsenate (As_i; Fig. 8). For large Ca^{2+} additions (Fig. 8, A–E), the most obvious effect of substituting P_i was that the total Ca^{2+} load at which PTP was triggered was markedly lower with V_i or As_i, as indicated by loss of the ability to retain matrix Ca^{2+} (Fig. 8, A and B), $\Delta\Psi_m$ depolarization (Fig. 8 C), and rapid mitochondrial swelling (Fig. 8 D). Interestingly, this PTP sensitization could not be directly attributed to differences in $[Ca^{2+}]_{mito}$; V_i substitution lowered $[Ca^{2+}]_{mito}$ and substantially decreased the rate of mitochondrial Ca^{2+} uptake, whereas As_i potentiated $[Ca^{2+}]_{mito}$ without having a significant effect on the uptake rate. Matrix Ca^{2+} buffering, as indicated by the bound/free Ca^{2+} ratio (Fig. 8 E), was more effective for V_i and less effective for As_i for the first few Ca^{2+} additions, as compared with P_i, although just before the activation of PTP in V_i and As_i, bound/free Ca^{2+} was similar for all three anions. Striking differences in the extent of $\Delta\Psi_m$ depolarization during Ca^{2+} uptake were evident when P_i was substituted with As_i or V_i (Fig. 8 C). V_i substitution had the largest effect, causing a $\Delta\Psi_m$ depolarization of >30 mV after the first Ca^{2+} addition, whereas the depolarization was only 2 mV in P_i. With smaller Ca^{2+} additions, there was little effect of

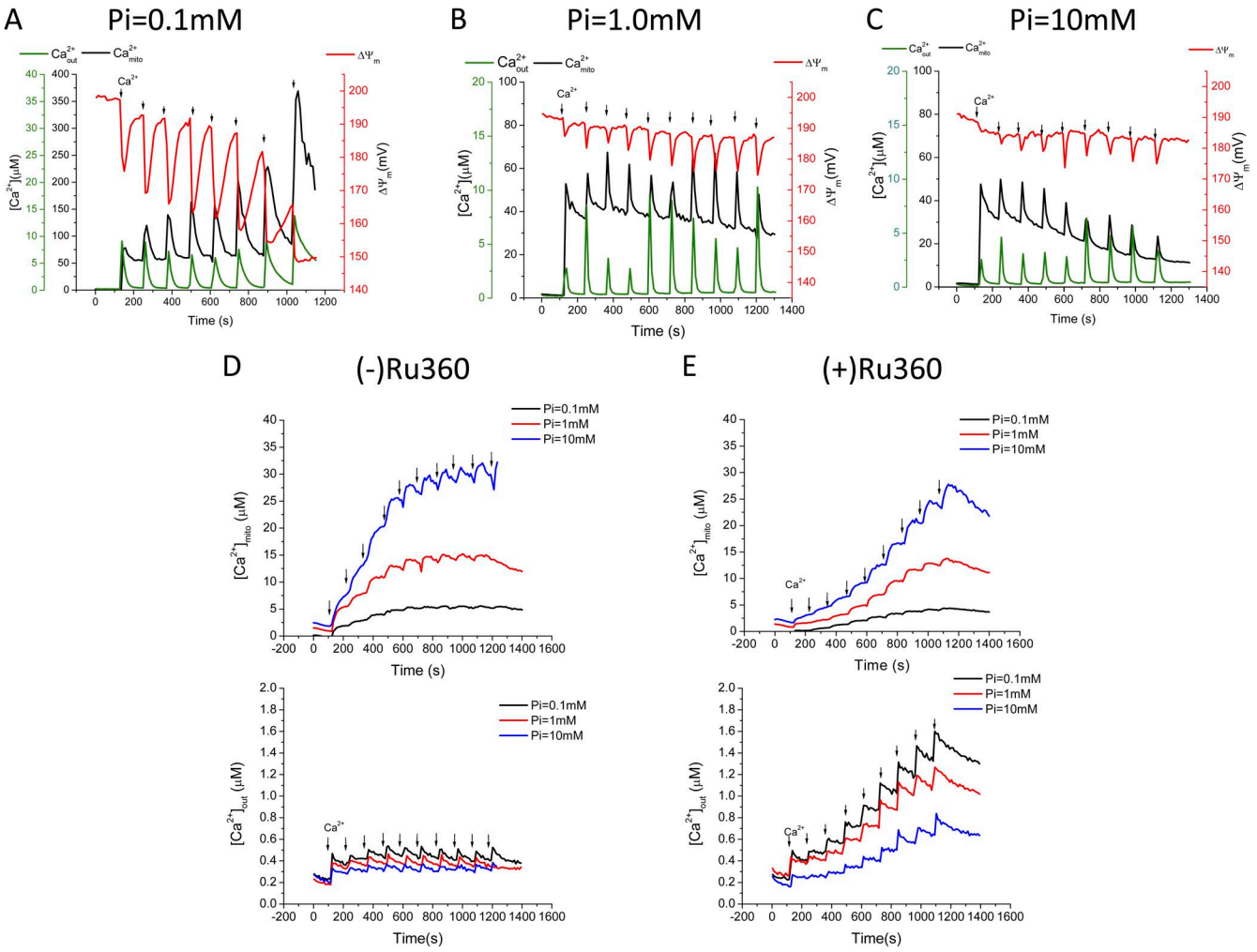

Figure 7. Inorganic phosphate (P_i) dependence of mitochondrial Ca^{2+} uptake for large or small Ca^{2+} additions. Isolated mitochondria were incubated in 0.1 (A), 1 (B), or 10 (C) mM P_i with 5 mM NaCl, 5 mM G/M, and 1 µM CsA present. Ca^{2+} additions: First Ca^{2+} addition was 15.3 µM, subsequent additions 5.7 µM each (A–C); red line represents mitochondrial membrane potential $\Delta\Psi$ (D–E). First Ca^{2+} addition 0.2 µM, subsequent 0.011 µM each. The black, red, blue lines represent 0.1, 1.0, and 10.0 mM P_i, respectively. (E) 10 nM Ru360-treated mitochondria.

anion substitution on the $\Delta\Psi_m$ (Fig. 8 H) or light scattering responses (Fig. 8 I), but just as for the larger Ca^{2+} pulses, $[Ca^{2+}]_{mito}$ was lower in V_i.

DISCUSSION

In the present work, we used calibrated Ca^{2+}-sensitive fluorescent indicators to quantitatively measure changes in $[Ca^{2+}]_{out}$ and $[Ca^{2+}]_{mito}$ (as well as $\Delta\Psi_m$ and light scattering in some experiments) during mitochondrial Ca^{2+} uptake in isolated mitochondria. This method allowed us to identify two components of Ca^{2+} influx that have: (1) very different effects on matrix free $[Ca^{2+}]$, (2) different sensitivities to inhibition by Ru360, (3) different affinities for Ca^{2+}, and (4) different responses to a change in P_i. MCU_{mode1} required at least 1 µM Ru360 to be completely inhibited, and responded to small Ca^{2+} additions in the range of 0.1 to 2 µM with rapid and large changes in $[Ca^{2+}]_{mito}$. MCU_{mode2} was blocked by <100 nM Ru360, was responsible for the bulk of total Ca^{2+} uptake for large Ca^{2+} additions in the range of 2 to 15 µM, and took >100 s to reach steady state. The finding that the MCU_{mode1} could mediate changes in $[Ca^{2+}]_{mito}$ of 10 s of µM, even in the presence of 100 nM Ru360, indicates that at low total Ca^{2+} loads there is a finite degree of Ca^{2+} buffering in the matrix; however, at the much higher Ca^{2+} loads supported by MCU_{mode2}, a secondary dynamic Ca^{2+} buffering system involving P_i is engaged. The results suggest that the role of MCU_{mode1} might be to modulate oxidative phosphorylation in response to intracellular Ca^{2+} signaling, whereas MCU_{mode2}, and the dynamic high-capacity Ca^{2+} buffering system constitutes a Ca^{2+} sink function. Interestingly, the trigger for PTP activation is unlikely to be $[Ca^{2+}]_{mito}$ itself but rather a downstream byproduct of matrix Ca^{2+} loading.

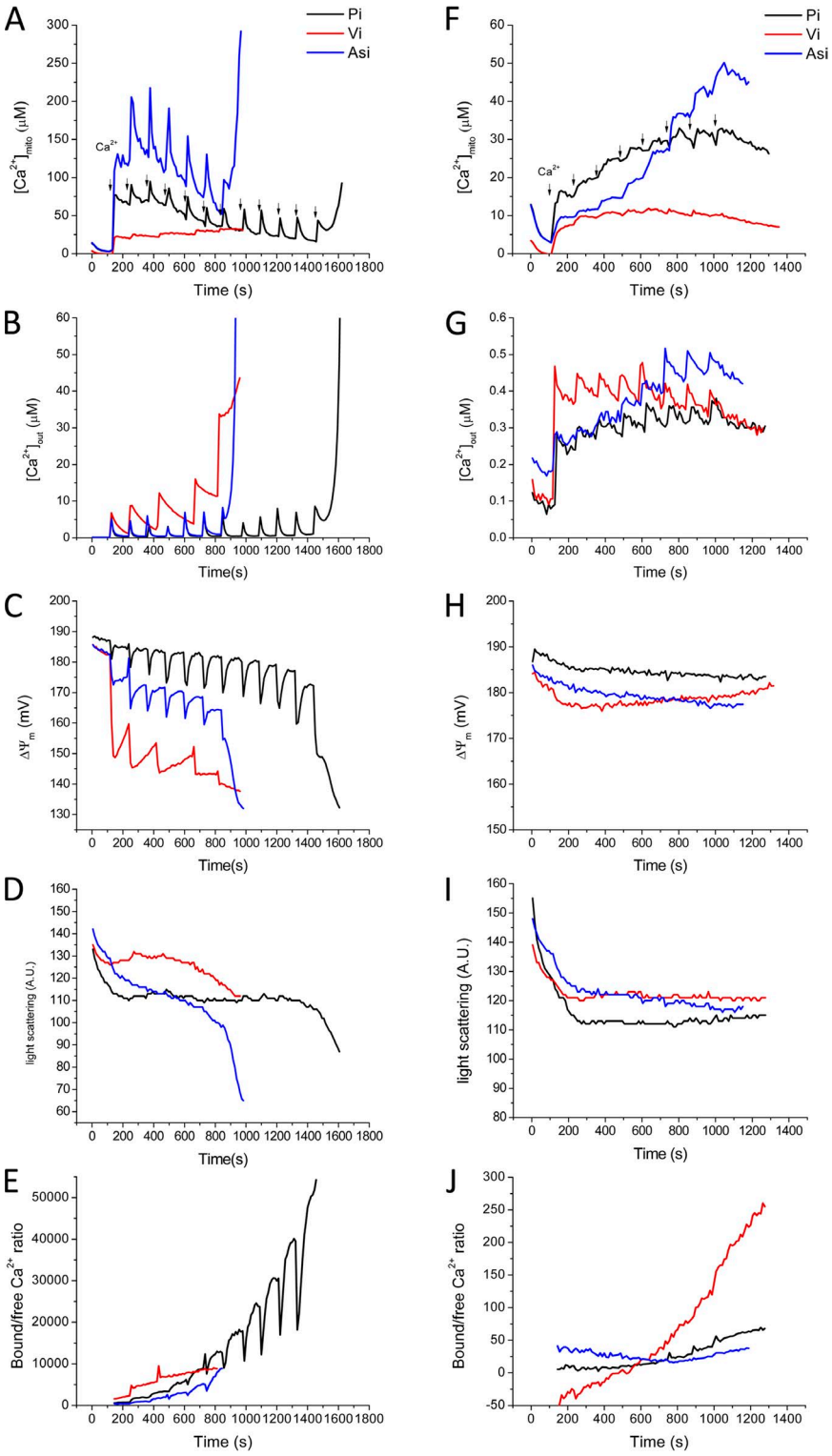

Figure 8. Effects of $P_{i,}$ (black), arsenate (As_i, blue), or vanadate (V_i, red) anions on the regulation of mitochondrial Ca^{2+}. The buffer solution contained 2 mM P_i, As_i, or V_i in the presence of 1 μM of CsA. (A–E) Large Ca^{2+} additions (first Ca^{2+} addition was 15.3 μM, subsequent additions 5.7 μM each) were made until mitochondrial PTP opening occurred, as indicated by $\Delta\Psi_m$ collapse (C), swelling (D), and uncontrolled Ca^{2+} efflux (A). (F–J) Smaller Ca^{2+} additions (first Ca^{2+} addition 0.2 μM, subsequent 0.011 μM each) evoked similar $[Ca^{2+}]_{mito}$ responses without significantly disrupting $\Delta\Psi_m$ or activating PTP.

Several earlier studies have used AM loading of Ca^{2+} indicators in isolated mitochondria to qualitatively assess matrix Ca^{2+} responses (Davis et al., 1987; Lukács and Kapus, 1987; Gunter et al., 1988; Lukács et al., 1988). A key question that one must first answer before interpretations about matrix Ca^{2+} can be made is whether the dye is localized exclusively in the matrix, or if a certain fraction of the signal is coming from a nonmatrix compartment. Our evidence conclusively demonstrates that the fura-FF is reporting matrix Ca^{2+}. Both the fast and slow components of the $[Ca^{2+}]_{mito}$ signal can be completely blocked by Ru360, albeit with different sensitivities. In the case of MCU_{mode1} in particular, the kinetics were slowed by Ru360 in a concentration-dependent

manner (Fig. 3 B). The initial rate of rise of MCU_{mode1} was approximately one order of magnitude slower in 100 nM Ru360 for a range of Ca^{2+} additions (Fig. 4). In addition, the depolarization of $\Delta\Psi_m$ upon Ca^{2+} addition tracks the rapid component of the $[Ca^{2+}]_{mito}$ response. This dissipation of the protonmotive force can occur only when Ca^{2+} current is flowing across the inner membrane. Fourth, when $[Ca^{2+}]_{out}$ is lowered by EGTA addition to the cuvette, $[Ca^{2+}]_{mito}$ remains high (Fig. 5 A) in the absence of Na^+ because the mNCE is disabled, but it declines when mNCE is functional (Fig. 5 B). Thus, all of the evidence is consistent with matrix localization of the fura-FF.

Rapid effects of Ca^{2+} on mitochondrial function have been known since 1965 when Chance (1965) reported that Ca^{2+} was able to induce a "state 4 to state 3" respiratory transition in a manner similar to, but slightly faster than, ADP. Ca^{2+} addition (200 µM) by means of a rapid mixing device caused a cytochrome b oxidation response with a halftime of 70 ms. Territo et al. (2001) showed that the initial response time of mitochondrial Ca^{2+}-stimulated respiration and light scattering changes is <300 ms for Ca^{2+} additions in the range of ∼60 to 2,000 nM and also reported that a 535-nM Ca^{2+} addition increased $[Ca^{2+}]_{mito}$ by ∼700 nM (as measured using Rhod-2). Gunter and Pfeiffer (1990) and Sparagna et al. (1995) proposed that two pathways for mitochondrial Ca^{2+} uptake exist, a RaM which responds to fast transients of Ca^{2+} in the physiological range (100–500 nM) and the classical MCU which has a low affinity and slow kinetics. RaM-mediated uptake was complete in only 0.3 s and was inactivated when the prepulse steady-state Ca^{2+} exceeded 150 nM. Its amplitude could be fully reset after 1 min in <100 nM Ca^{2+} in cardiac mitochondria (Buntinas et al., 2001). Interestingly, RaM was found to be less sensitive to Ruthenium red than MCU (Sparagna et al., 1995; Buntinas et al., 2001). Hence, several aspects of MCU_{mode1} in the present study are similar to the properties of RaM, for example, a lower sensitivity to Ru360 and a higher Ca^{2+} affinity than MCU_{mode2}. However, in the present study, MCU_{mode1} kinetics were slower to reach steady state. For example, in Fig. 2 E, there is a very rapid component of initial uptake for a Ca^{2+} addition of 200 nM, but $[Ca^{2+}]_{mito}$ was still increasing 100 s after the addition and did not appear to be inactivated in the way that RaM would be when subsequent Ca^{2+} additions were made (Fig. 2 F).

Whether MCU_{mode1} and MCU_{mode2} are two modes of the same Ca^{2+} channel or are separate proteins remains to be determined. The recent discovery that knockdown of the product of the gene CCDC109A (renamed MCU) suppresses MCU_{mode2} (Baughman et al., 2011; De Stefani et al., 2011) might allow us to answer this question in future studies. Nevertheless, two Ca^{2+} channels (mCa1 and mCa2) with different gating and conductance properties have been observed recently in mitoplast patch clamp studies of cardiac mitochondria (Michels et al., 2009). MCa1 was inhibited by 200 nM Ru360, whereas mCa2, which had a lower conductance, required 10 µM Ru360 to be suppressed, providing some evidence to suggest that two independent Ca^{2+} channels with different Ru360 sensitivities exist in the inner membrane. The skeletal muscle isoform of the ryanodine receptor has also been proposed as an alternative mitochondrial Ca^{2+} uptake protein. We did not observe any effect of 100 µM ryanodine on Ca^{2+} uptake kinetics in our experiments (Fig. S2).

The remarkable finding of the present study was that small amounts of Ca^{2+} uptake lead to large changes in $[Ca^{2+}]_{mito}$, whereas large Ca^{2+} additions give only a transient increase in $[Ca^{2+}]_{mito}$ with no change or an even a lower steady-state Ca^{2+}. Two possible explanations could account for the paradoxical behavior of $[Ca^{2+}]_{mito}$; either the Ca^{2+} efflux rate from the mitochondria increases to match the Ca^{2+} entering for large Ca^{2+} loads, or Ca^{2+} buffering in the matrix is markedly increased in parallel with Ca^{2+} entry. The former explanation can be ruled out because we simultaneously measured $[Ca^{2+}]_{out}$, which confirmed that the Ca^{2+} taken up was retained inside the mitochondria. Under zero Na^+ conditions, or in the presence of CGP-37157, an inhibitor of mNCE, $[Ca^{2+}]_{mito}$, was minimally affected (Fig. S3), although there was an effect of Na^+ on the extramitochondrial Ca^{2+} steady-state concentration, as we have previously described (Wei et al., 2011). The only remaining explanation is that above a certain threshold of Ca^{2+} uptake, the Ca^{2+} buffer capacity increases rapidly to counteract MCU_{mode2}-mediated uptake. This behavior is similar to that reported by Chalmers and Nicholls (2003) for rat liver and brain mitochondria. They noted that, over a wide range of mitochondrial Ca^{2+} loads (from 10 to 500 nmol/mg), mitochondria were capable of maintaining $[Ca^{2+}]_{mito}$ within a narrow range between 1 and 5 µM, whereas <10 nmol/mg $[Ca^{2+}]_{mito}$ was more linearly related to the magnitude of the uptake. Because the dynamic buffering occurred in the presence of P_i, but not when acetate was the anion, they interpreted the buffering mechanism to be related to the formation of calcium-phosphate complexes, in accordance with other studies (David, 1999; Nicholls, 2005; Warashina, 2006). Our data are consistent with this interpretation but differ in the quantitative details. For small Ca^{2+} additions, $[Ca^{2+}]_{mito}$ increased in a stepwise manner from a baseline of ∼2.5 µM up to ∼25 µM before the secondary buffering took effect and a plateau was reached (Fig. 2 E). This corresponded to an increase in calcium-phosphate buffering occurring after a total Ca^{2+} load of 0.5 nmol/mg (Fig. 2 G). This threshold is likely to vary depending on how the Ca^{2+} addition is made. For example, the larger additions evoked only a single rapid jump in $[Ca^{2+}]_{mito}$ to ∼60 µM (Fig. 2 A) at a total load of 25 nmol/mg, followed by more and more efficient buffering up to 100 nmol/mg (Fig. 2 C). The bound/free Ca^{2+} ratio increased continuously to a level

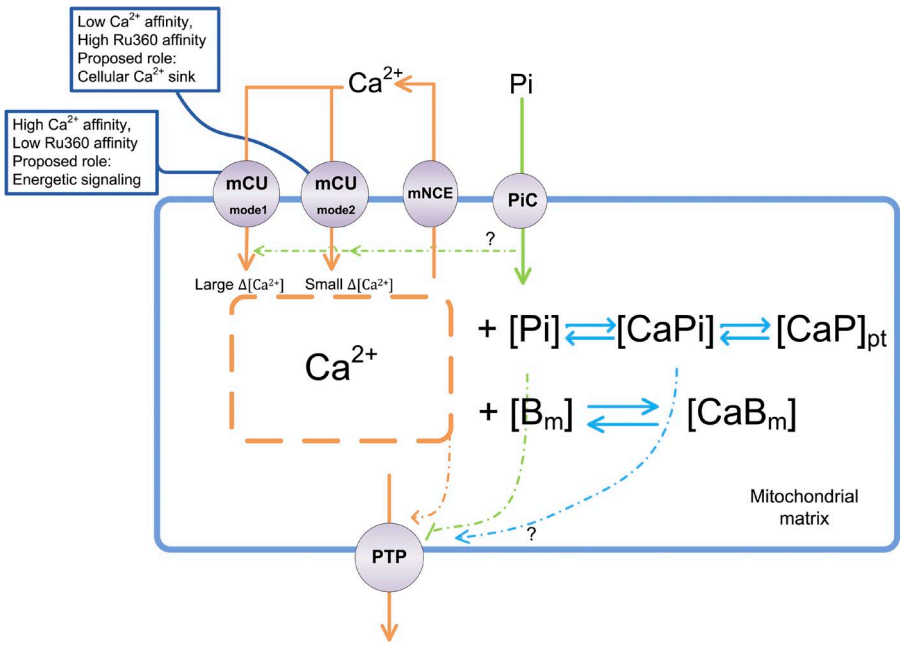

Figure 9. Summary of the mechanisms governing mitochondrial Ca^{2+} dynamics. Mitochondrial Ca^{2+} uptake occurs through MCU_{mode1} with a high Ca^{2+} affinity, but low Ru360 sensitivity, whereas the bulk of mitochondrial Ca^{2+} loading occurs through the low Ca^{2+} affinity, high Ru360-sensitive MCU_{mode2}. Ca^{2+} extrusion occurs through the mNCE. Rapid Ca^{2+} entry via MCU_{mode1} saturates fixed mitochondrial Ca^{2+} buffers (B_m) to produce a large change in $[Ca^{2+}]_{mito}$, whereas larger amounts of Ca^{2+} entry, along with P_i uptake, result in reversible precipitation of calcium-phosphate (CaP_{pt}) with little effect on steady-state $[Ca^{2+}]_{mito}$. P_i is transported into mitochondria through the phosphate carrier (PiC). Mitochondrial matrix contents are released when the mitochondrial PTP opens. PTP opening correlates with total mitochondrial Ca^{2+} load but not $[Ca^{2+}]_{mito}$, perhaps through the formation of calcium-phosphate complexes.

>30,000 as ΣCa^{2+}_{uptake} increased. Increasing P_i over a range from 0.1 to 10 mM did, in fact, result in a lower steady-state $[Ca^{2+}]_{mito}$ for large Ca^{2+} additions (Fig. 7, A–C). In addition, at 0.1 mM P_i, the rate of Ca^{2+} uptake through MCU_{mode2} was markedly depressed, $\Delta\Psi_m$ depolarization was deeper and slower to recover, and $[Ca^{2+}]_{mito}$ rose dramatically for the later Ca^{2+} additions. The slower kinetics of MCU_{mode2} in 0.1 mM P_i could be related to a decreased rate of calcium-phosphate formation, which would limit the influx rate by decreasing the electrochemical driving force for Ca^{2+} entry, or it could be a result of the Ca^{2+} influx rate being limited by the slow kinetics of the P_i transport process because anion flux would be required to maintain electroneutrality during movement of the divalent cation. In contrast to the P_i effect on large Ca^{2+} additions, P_i enhanced the rise in $[Ca^{2+}]_{mito}$ with each small Ca^{2+} addition. This was the result of enhanced total Ca^{2+} uptake rather than a change in matrix buffering, as indicated by lower $[Ca^{2+}]_{out}$ at high P_i (Fig. 7, D and E). Facilitation of MCU_{mode1} by P_i was even present when MCU_{mode2} was blocked by Ru360.

Substitution of P_i with As_i or V_i had striking effects on $[Ca^{2+}]_{mito}$ and the threshold for PTP activation. Interestingly, As_i and V_i had opposite effects on $[Ca^{2+}]_{mito}$ for multiple pulses but they both sensitized the mitochondria to PTP activation. Although As_i appeared to substitute reasonably well for P_i for the first six Ca^{2+} additions with respect to the overall kinetics of MCU_{mode2}, V_i substitution slowed Ca^{2+} uptake and inhibited the rise in $[Ca^{2+}]_{mito}$. Even though the total Ca^{2+} uptake was lower in V_i, the PTP activation threshold was the lowest of the three anions. In accord with the conclusions of Chalmers and Nicholls (2003), PTP activation was, in all cases, independent of $[Ca^{2+}]_{mito}$. Therefore, an alternative hypothesis is required to explain why the PTP is activated at a reproducible total mitochondrial Ca^{2+} load. One possible mechanism could be related to the formation of Ca^{2+}-phosphate species or Ca^{2+}-polyphosphate complexes (Pavlov et al., 2005; Abramov et al., 2007). If this is the case, both As_i and V_i appear to be adequate (or better) substitutes for P_i in terms of triggering PTP. Recently, Basso et al. (2008) reported that the desensitizing effect of CsA on PTP activation by Ca^{2+} is absent when As_i or V_i are substituted for P_i. Our results confirm this finding and argue against the potential explanation that differences in Ca^{2+} buffering and $[Ca^{2+}]_{mito}$ could be behind the As_i and V_i effects.

Based on the experimental observations, we propose that mechanisms of mitochondrial Ca^{2+} uptake and matrix Ca^{2+} buffering involve two stages (summarized in Fig. 9): (1) Ca^{2+} uptake mediated by MCU_{mode1} for extramitochondrial Ca^{2+} changes in the physiological range of cytoplasmic Ca^{2+} that lead to a rise in $[Ca^{2+}]_{mito}$ as the fixed Ca^{2+} buffers become saturated, and (2) Ca^{2+} uptake mediated by MCU_{mode2} that is accompanied by rapid buffering via calcium-phosphate complex formation with little change in $[Ca^{2+}]_{mito}$. Importantly, the MCU_{mode1} pathway would be accelerated by nearby Ca^{2+} release into a local extramitochondrial microdomain (Hajnóczky et al., 2000), explaining observations of rapidly rising mitochondrial Ca^{2+} transients during cardiac excitation-contraction coupling (Maack et al., 2006). The magnitude of changes in $[Ca^{2+}]_{mito}$ brought about by MCU_{mode1} would fulfill the role of a signal to increase oxidative phosphorylation and ATP production (Bell et al., 2006), as they span the range of activation of the Ca^{2+} dependent dehydrogenases, pyruvate dehydrogenase, α-ketoglutarate dehydrogenase, and isocitrate

dehydrogenase (McCormack et al., 1990), and/or Ca^{2+}-dependent allosteric regulatory sites on the respiratory chain complexes (Territo et al., 2000). In contrast, MCU_{mode2}, along with the rapid dynamic Ca^{2+} buffering mechanism, fulfills the role of a protective Ca^{2+} sink for the cell, enabling the cell to survive in the presence of rather large total Ca^{2+} loads, for example, those that might be encountered in the heart during ischemia-reperfusion, tachycardia, or maximal sympathetic stimulation. In this scenario, the major mitochondrial Ca^{2+} efflux pathway, mNCE, would serve as a modulator of the balance between cytoplasmic Ca^{2+} and matrix Ca^{2+} because its capacity to counteract large MCU fluxes is limited (and would tend to cause cytoplasmic Ca^{2+} overload if its Vmax was fast enough to match MCU-mediated influx). PTP activation can be clearly dissociated from $[Ca^{2+}]_{mito}$ overload by itself but does correlate well with a reproducible threshold of total mitochondrial Ca^{2+} loading. This suggests that a downstream by-product of Ca^{2+}, perhaps a Ca^{2+}-phosphate species itself, triggers permeabilization of the inner membrane. How cyclophilin D modulates this trigger remains a mystery because it seems that substitution of P_i with As_i or V_i bypasses the inhibition by cyclosporin A.

In conclusion, understanding mitochondrial Ca^{2+} dynamics requires quantitative assessment of not only Ca^{2+} influx and efflux rates across the mitochondria, but rates of matrix Ca^{2+} buffering at different Ca^{2+} loads and rates of entry. The future development of computational models that incorporate all of these factors will help us understand these interesting features that are vitally important for Ca^{2+} homeostasis, cell death, and cardiac disease.

This work was supported by National Institutes of Health grants R01HL101235 and R37HL54598 (to B. O'Rourke) and R01HL105216 (to R.L. Winslow).

Edward N. Pugh Jr. served as editor.

Submitted: 28 February 2012
Accepted: 2 May 2012

REFERENCES

Abramov, A.Y., C. Fraley, C.T. Diao, R. Winkfein, M.A. Colicos, M.R. Duchen, R.J. French, and E. Pavlov. 2007. Targeted polyphosphatase expression alters mitochondrial metabolism and inhibits calcium-dependent cell death. *Proc. Natl. Acad. Sci. USA.* 104:18091–18096. http://dx.doi.org/10.1073/pnas.0708959104

Andrienko, T.N., E. Picht, and D.M. Bers. 2009. Mitochondrial free calcium regulation during sarcoplasmic reticulum calcium release in rat cardiac myocytes. *J. Mol. Cell. Cardiol.* 46:1027–1036. http://dx.doi.org/10.1016/j.yjmcc.2009.03.015

Aon, M.A., S. Cortassa, A.C. Wei, M. Grunnet, and B. O'Rourke. 2010. Energetic performance is improved by specific activation of K+ fluxes through K(Ca) channels in heart mitochondria. *Biochim. Biophys. Acta.* 1797:71–80.

Basso, E., V. Petronilli, M.A. Forte, and P. Bernardi. 2008. Phosphate is essential for inhibition of the mitochondrial permeability transition pore by cyclosporin A and by cyclophilin D ablation. *J. Biol. Chem.* 283:26307–26311. http://dx.doi.org/10.1074/jbc.C800132200

Baughman, J.M., F. Perocchi, H.S. Girgis, M. Plovanich, C.A. Belcher-Timme, Y. Sancak, X.R. Bao, L. Strittmatter, O. Goldberger, R.L. Bogorad, et al. 2011. Integrative genomics identifies MCU as an essential component of the mitochondrial calcium uniporter. *Nature.* 476:341–345. http://dx.doi.org/10.1038/nature10234

Bell, C.J., N.A. Bright, G.A. Rutter, and E.J. Griffiths. 2006. ATP regulation in adult rat cardiomyocytes: time-resolved decoding of rapid mitochondrial calcium spiking imaged with targeted photoproteins. *J. Biol. Chem.* 281:28058–28067. http://dx.doi.org/10.1074/jbc.M604540200

Beutner, G., V.K. Sharma, D.R. Giovannucci, D.I. Yule, and S.S. Sheu. 2001. Identification of a ryanodine receptor in rat heart mitochondria. *J. Biol. Chem.* 276:21482–21488. http://dx.doi.org/10.1074/jbc.M101486200

Bragadin, M., T. Pozzan, and G.F. Azzone. 1979. Kinetics of Ca2+ carrier in rat liver mitochondria. *Biochemistry.* 18:5972–5978. http://dx.doi.org/10.1021/bi00593a033

Buntinas, L., K.K. Gunter, G.C. Sparagna, and T.E. Gunter. 2001. The rapid mode of calcium uptake into heart mitochondria (RaM): comparison to RaM in liver mitochondria. *Biochim. Biophys. Acta.* 1504:248–261. http://dx.doi.org/10.1016/S0005-2728(00)00254-1

Chalmers, S., and D.G. Nicholls. 2003. The relationship between free and total calcium concentrations in the matrix of liver and brain mitochondria. *J. Biol. Chem.* 278:19062–19070. http://dx.doi.org/10.1074/jbc.M212661200

Chance, B. 1965. The energy-linked reaction of calcium with mitochondria. *J. Biol. Chem.* 240:2729–2748.

Chinopoulos, C., and V. Adam-Vizi. 2010. Mitochondrial Ca2+ sequestration and precipitation revisited. *FEBS J.* 277:3637–3651. http://dx.doi.org/10.1111/j.1742-4658.2010.07755.x

Crompton, M. 1999. The mitochondrial permeability transition pore and its role in cell death. *Biochem. J.* 341:233–249. http://dx.doi.org/10.1042/0264-6021:3410233

Crompton, M., F. Palmieri, M. Capano, and E. Quagliariello. 1975. A kinetic study of sulphate transport in rat liver mitochondria. *Biochem. J.* 146:667–673.

Crompton, M., M. Künzi, and E. Carafoli. 1977. The calcium-induced and sodium-induced effluxes of calcium from heart mitochondria. Evidence for a sodium-calcium carrier. *Eur. J. Biochem.* 79:549–558. http://dx.doi.org/10.1111/j.1432-1033.1977.tb11839.x

David, G. 1999. Mitochondrial clearance of cytosolic Ca(2+) in stimulated lizard motor nerve terminals proceeds without progressive elevation of mitochondrial matrix [Ca(2+)]. *J. Neurosci.* 19:7495–7506.

Davis, M.H., R.A. Altschuld, D.W. Jung, and G.P. Brierley. 1987. Estimation of intramitochondrial pCa and pH by fura-2 and 2,7 biscarboxyethyl-5(6)-carboxyfluorescein (BCECF) fluorescence. *Biochem. Biophys. Res. Commun.* 149:40–45. http://dx.doi.org/10.1016/0006-291X(87)91602-0

De Stefani, D., A. Raffaello, E. Teardo, I. Szabò, and R. Rizzuto. 2011. A forty-kilodalton protein of the inner membrane is the mitochondrial calcium uniporter. *Nature.* 476:336–340. http://dx.doi.org/10.1038/nature10230

Deber, C.M., J. Tom-Kun, E. Mack, and S. Grinstein. 1985. Bromo-A23187: a nonfluorescent calcium ionophore for use with fluorescent probes. *Anal. Biochem.* 146:349–352. http://dx.doi.org/10.1016/0003-2697(85)90550-0

Demaurex, N., and C. Distelhorst. 2003. Cell biology. Apoptosis—the calcium connection. *Science.* 300:65–67. http://dx.doi.org/10.1126/science.1083628

Denton, R.M., J.G. McCormack, and N.J. Edgell. 1980. Role of calcium ions in the regulation of intramitochondrial metabolism.

Effects of Na+, Mg2+ and ruthenium red on the Ca2+-stimulated oxidation of oxoglutarate and on pyruvate dehydrogenase activity in intact rat heart mitochondria. *Biochem. J.* 190:107–117.

Elrod, J.W., R. Wong, S. Mishra, R.J. Vagnozzi, B. Sakthievel, S.A. Goonasekera, J. Karch, S. Gabel, J. Farber, T. Force, et al. 2010. Cyclophilin D controls mitochondrial pore-dependent Ca(2+) exchange, metabolic flexibility, and propensity for heart failure in mice. *J. Clin. Invest.* 120:3680–3687. http://dx.doi.org/10.1172/JCI43171

Grynkiewicz, G., M. Poenie, and R.Y. Tsien. 1985. A new generation of Ca2+ indicators with greatly improved fluorescence properties. *J. Biol. Chem.* 260:3440–3450.

Gunter, T.E., and D.R. Pfeiffer. 1990. Mechanisms by which mitochondria transport calcium. *Am. J. Physiol.* 258:C755–C786.

Gunter, T.E., D. Restrepo, and K.K. Gunter. 1988. Conversion of esterified fura-2 and indo-1 to Ca2+-sensitive forms by mitochondria. *Am. J. Physiol.* 255:C304–C310.

Hajnóczky, G., G. Csordás, M. Madesh, and P. Pacher. 2000. The machinery of local Ca2+ signalling between sarco-endoplasmic reticulum and mitochondria. *J. Physiol.* 529:69–81. http://dx.doi.org/10.1111/j.1469-7793.2000.00069.x

Kirichok, Y., G. Krapivinsky, and D.E. Clapham. 2004. The mitochondrial calcium uniporter is a highly selective ion channel. *Nature.* 427:360–364. http://dx.doi.org/10.1038/nature02246

Kohlhaas, M., T. Liu, A. Knopp, T. Zeller, M.F. Ong, M. Böhm, B. O'Rourke, and C. Maack. 2010. Elevated cytosolic Na+ increases mitochondrial formation of reactive oxygen species in failing cardiac myocytes. *Circulation.* 121:1606–1613. http://dx.doi.org/10.1161/CIRCULATIONAHA.109.914911

Liu, T., and B. O'Rourke. 2008. Enhancing mitochondrial Ca2+ uptake in myocytes from failing hearts restores energy supply and demand matching. *Circ. Res.* 103:279–288. http://dx.doi.org/10.1161/CIRCRESAHA.108.175919

Lukács, G.L., and A. Kapus. 1987. Measurement of the matrix free Ca2+ concentration in heart mitochondria by entrapped fura-2 and quin2. *Biochem. J.* 248:609–613.

Lukács, G.L., A. Kapus, and A. Fonyó. 1988. Parallel measurement of oxoglutarate dehydrogenase activity and matrix free Ca2+ in fura-2-loaded heart mitochondria. *FEBS Lett.* 229:219–223. http://dx.doi.org/10.1016/0014-5793(88)80831-7

Maack, C., and B. O'Rourke. 2007. Excitation-contraction coupling and mitochondrial energetics. *Basic Res. Cardiol.* 102:369–392. http://dx.doi.org/10.1007/s00395-007-0666-z

Maack, C., S. Cortassa, M.A. Aon, A.N. Ganesan, T. Liu, and B. O'Rourke. 2006. Elevated cytosolic Na+ decreases mitochondrial Ca2+ uptake during excitation-contraction coupling and impairs energetic adaptation in cardiac myocytes. *Circ. Res.* 99:172–182. http://dx.doi.org/10.1161/01.RES.0000232546.92777.05

McCormack, J.G., A.P. Halestrap, and R.M. Denton. 1990. Role of calcium ions in regulation of mammalian intramitochondrial metabolism. *Physiol. Rev.* 70:391–425.

Michels, G., I.F. Khan, J. Endres-Becker, D. Rottlaender, S. Herzig, A. Ruhparwar, T. Wahlers, and U.C. Hoppe. 2009. Regulation of the human cardiac mitochondrial Ca2+ uptake by 2 different voltage-gated Ca2+ channels. *Circulation.* 119:2435–2443. http://dx.doi.org/10.1161/CIRCULATIONAHA.108.835389

Nicholls, D.G. 2005. Mitochondria and calcium signaling. *Cell Calcium.* 38:311–317. http://dx.doi.org/10.1016/j.ceca.2005.06.011

Nicholls, D.G., and S. Chalmers. 2004. The integration of mitochondrial calcium transport and storage. *J. Bioenerg. Biomembr.* 36:277–281. http://dx.doi.org/10.1023/B:JOBB.0000041753.52832.f3

Palty, R., W.F. Silverman, M. Hershfinkel, T. Caporale, S.L. Sensi, J. Parnis, C. Nolte, D. Fishman, V. Shoshan-Barmatz, S. Herrmann, et al. 2010. NCLX is an essential component of mitochondrial Na+/Ca2+ exchange. *Proc. Natl. Acad. Sci. USA.* 107:436–441. http://dx.doi.org/10.1073/pnas.0908099107

Pavlov, E., E. Zakharian, C. Bladen, C.T. Diao, C. Grimbly, R.N. Reusch, and R.J. French. 2005. A large, voltage-dependent channel, isolated from mitochondria by water-free chloroform extraction. *Biophys. J.* 88:2614–2625. http://dx.doi.org/10.1529/biophysj.104.057281

Ryu, S.Y., G. Beutner, R.T. Dirksen, K.W. Kinnally, and S.S. Sheu. 2010. Mitochondrial ryanodine receptors and other mitochondrial Ca2+ permeable channels. *FEBS Lett.* 584:1948–1955. http://dx.doi.org/10.1016/j.febslet.2010.01.032

Saavedra-Molina, A., S. Uribe, and T.M. Devlin. 1990. Control of mitochondrial matrix calcium: studies using fluo-3 as a fluorescent calcium indicator. *Biochem. Biophys. Res. Commun.* 167:148–153. http://dx.doi.org/10.1016/0006-291X(90)91743-C

Scaduto, R.C. Jr., and L.W. Grotyohann. 1999. Measurement of mitochondrial membrane potential using fluorescent rhodamine derivatives. *Biophys. J.* 76:469–477. http://dx.doi.org/10.1016/S0006-3495(99)77214-0

Sparagna, G.C., K.K. Gunter, S.S. Sheu, and T.E. Gunter. 1995. Mitochondrial calcium uptake from physiological-type pulses of calcium. A description of the rapid uptake mode. *J. Biol. Chem.* 270:27510–27515. http://dx.doi.org/10.1074/jbc.270.46.27510

Szabadkai, G., and M.R. Duchen. 2008. Mitochondria: the hub of cellular Ca2+ signaling. *Physiology (Bethesda).* 23:84–94. http://dx.doi.org/10.1152/physiol.00046.2007

Szanda, G., A. Rajki, S. Gallego-Sandín, J. Garcia-Sancho, and A. Spät. 2009. Effect of cytosolic Mg2+ on mitochondrial Ca2+ signaling. *Pflugers Arch.* 457:941–954. http://dx.doi.org/10.1007/s00424-008-0551-0

Territo, P.R., V.K. Mootha, S.A. French, and R.S. Balaban. 2000. Ca(2+) activation of heart mitochondrial oxidative phosphorylation: role of the F(0)/F(1)-ATPase. *Am. J. Physiol. Cell Physiol.* 278:C423–C435.

Territo, P.R., S.A. French, M.C. Dunleavy, F.J. Evans, and R.S. Balaban. 2001. Calcium activation of heart mitochondrial oxidative phosphorylation: rapid kinetics of mVO2, NADH, AND light scattering. *J. Biol. Chem.* 276:2586–2599. http://dx.doi.org/10.1074/jbc.M002923200

Walajtys-Rhode, E., J. Zapatero, G. Moehren, and J.B. Hoek. 1992. The role of the matrix calcium level in the enhancement of mitochondrial pyruvate carboxylation by glucagon pretreatment. *J. Biol. Chem.* 267:370–379.

Wan, B., K.F. LaNoue, J.Y. Cheung, and R.C. Scaduto Jr. 1989. Regulation of citric acid cycle by calcium. *J. Biol. Chem.* 264:13430–13439.

Warashina, A. 2006. Mode of mitochondrial Ca2+ clearance and its influence on secretory responses in stimulated chromaffin cells. *Cell Calcium.* 39:35–46. http://dx.doi.org/10.1016/j.ceca.2005.09.001

Wei, A.C., T. Liu, S. Cortassa, R.L. Winslow, and B. O'Rourke. 2011. Mitochondrial Ca2+ influx and efflux rates in guinea pig cardiac mitochondria: low and high affinity effects of cyclosporine A. *Biochim. Biophys. Acta.* 1813:1373–1381. http://dx.doi.org/10.1016/j.bbamcr.2011.02.012

Ying, W.L., J. Emerson, M.J. Clarke, and D.R. Sanadi. 1991. Inhibition of mitochondrial calcium ion transport by an oxo-bridged dinuclear ruthenium ammine complex. *Biochemistry.* 30:4949–4952. http://dx.doi.org/10.1021/bi00234a016